CrossMark

NiCo$_2$O$_4$ grown on Co/C hybrid nanofiber film with excellent electrochemical performance for flexible supercapacitor electrodes

Chuan Fan[1] · Zongrong Ying[1] · Wenwen Zhang[1] · Tao Ju[1] · Bo Li[1]

Abstract

A flexible film electrode of NiCo$_2$O$_4$ grown on Co/C hybrid nanofibers (NCCNF) was synthesized through electrospinning combining with carbonization and hydrothermal reaction. X-ray diffraction, Raman spectroscopy, scanning electron microscopy and N$_2$ adsorption/desorption measurement were employed to characterize the composition, microstructure and morphology. The as-prepared flexible NCCNF film was used as a binder-free working electrode in three-electrode system and its electrochemical performance was evaluated by cyclic voltammetry, galvanostatic charge and discharge test and electrochemical impedance spectroscopy. The resulting flexible film shows excellent electrochemical performance with a high specific capacitance of up to 1710 F g^{-1} at 5 mV s^{-1}, making it a potentially practical electrode material for flexible supercapacitors.

1 Introduction

With the development of the world economy and technology, the demand for effective energy-storage devices grows accordingly. Due to their high power density, ultra-fast charge–discharge time, long cycling life and excellent reversibility, supercapacitors have drawn a lot of attention [1–4]. Compared with conventional rigid products, flexible and wearable electronics can significantly enhance consumers' daily use and maximize their compatibility with corresponding electronics [5, 6], thus flexible energy-storage devices have became a hot spot in both industry and academia [7, 8].

For flexible energy-storage devices, the key is appropriate flexible electrodes, about which many researches have been made over recent years [9–12]. Carbon nanotubes (CNTs)/graphene-based film electrodes are one of the predominant types of flexible electrodes, resulting from the high electro-activity, excellent electrical conductivity and super flexibility of CNTs and graphene [13–17]. Xiong et al. [13] reported a mechanically tough porous reduced graphene oxide film electrode prepared through a two-step process including blade-casting thin graphene oxide hydrogel films and reducing graphene oxide with hydriodic acid/acetic acid. Wu et al. [14] demonstrated a self-standing and flexible CNTs-based film electrodes fabricated via a simple vacuum-filtration procedure to one by one stack δ-MnO$_2$@CNTs composite layer and pure CNTs layer. Substrate-supported film electrodes are another main type of flexible electrodes, fabricated by growing active materials on inactive flexible substrates such as organic polymeric film [18], metal foil [19], and carbon fiber cloth [20, 21]. A highly flexible electrode, which is based on an electrodeposited-MnO$_2$/polypyrrole composite on a carbon cloth substrate, was reported [22] to possess a high specific capacitance of 325 F g^{-1} at a current density of 0.2 A g^{-1}, and an excellent rate capability with a capacitance retention of 70% at a high current density of 5.0 A g^{-1}. In addition, there are a few other researches [23–25] reported, for example, about conductive-polymer-based flexible hydrogel electrodes [26]. Wang et al. [27] exhibited a conducting polyaniline (PANI)-based flexible hydrogel electrode, which was synthesized by in situ embedding PANI within a chemically cross-linked PVA–H$_2$SO$_4$ hydrogel film with excellent elasticity, high mechanical strength, and ionic conductivity.

In the past decade, lots of researches have bee made on electrospun carbon or metal/carbon nanofiber film electrode materials [28–30]. However, only a few reports are presented on their flexible film electrodes [31–33]. Liu et al. [33] developed a highly flexible porous carbon nanofiber film,

✉ Zongrong Ying
  zrying@njust.edu.cn

1 School of Chemical Engineering, Nanjing University of Science and Technology, Nanjing 210094, People's Republic of China

which was fabricated by etching Co nanoparticles within electrospun Co/C hybrid nanofiber film without mechanical flexibility. In this work, we successfully synthesized a highly flexible Co/C hybrid nanofiber (CCNF) film through electrospinning followed by calcination, and furthermore, to achieve higher capacitance, a simple hydrothermal process was employed to further obtain flexible CCNF@NiCo$_2$O$_4$ (NCCNF) film. In our system, the existing Co plays a positive role in efficiently improving the mechanical flexibility and electrical conductivity of carbon matrix as well as providing some pseudocapacitive contributions. As we expected, the resulting flexible film exhibited excellent electrochemical performance with a specific capacitance of up to 1710 F g^{-1} at 5 mV s^{-1}, which is much higher than the previously reported value, and an about 70% remain of the initial capacitance after 1000 cycles at 1 A g^{-1}.

2 Materials and methods

2.1 Synthesis of CCNF film

In a typical process, 2.8 g of polyacrylonitrile (PAN) was dissolved in 20 ml of dimethyl formamide with vigorous stirring at 60 °C for 12 h. Then, 1.867 g of cobalt acetate tetrahydrate (Co(Ac)$_2 \cdot$ 4H$_2$O) was added to the above solution and vigorously stirred to finally form a homogeneous solution for electrospinning. The electrospinning process was performed with a spinning rate of 0.5 ml h^{-1} in a DC electric field of 1.33 kV m^{-1}, which was generated by applying a positive 20 kV voltage to a 15-cm gap between the needle and copper-net collector. Subsequently, after being dried at 60 °C for 2 h under vacuum to remove the residual solvent, the as-prepared electrospun film was first pre-oxidation in air at 260 °C for 1.5 h, and then carbonized under the atmosphere of nitrogen at 600 °C for 2 h with a heating rate of 1 °C min^{-1} to obtain CCNF film.

2.2 Synthesis of NCCNF film

A hydrothermal treatment was employed to load NiCo$_2$O$_4$ on the as-obtained CCNF film for preparing NCCNF film. 0.498 g of Co(Ac)$_2 \cdot$ 4H$_2$O and 0.248 g of Ni(Ac)$_2 \cdot$ 4H$_2$O were dissolved in 60 ml of deionized water. Then, a piece of 1 cm $\times$ 3 cm CCNF film was placed into the solution of Co(Ac)$_2$ and Ni(Ac)$_2$, and they were transferred into a 100 ml Teflon-lined stainless-steel autoclave and maintained at 90 °C for 5 h. After the autoclave being cooled down to room temperature, the resulting film was washed with deionized water and absolute alcohol several times, and then dried overnight at room temperature. Finally, the product was calcined in air at 250 °C for 3 h to get NCCNF film.

2.3 Characterization and electrochemical measurements

The crystal structure was characterized by a D8 Advance X-ray diffractometer (CuKα, 40 kV, 40 mA, λ = 1.5406 Å). The surface morphology and element composition were examined by a field scanning electron microscope (Model S-4800II) and a transmission electron microscopy (Model Tecnai G2 F30 S-Twin) coupled with an energy dispersive X-ray spectroscopy (EDS). All electrochemical measurements were carried out in a three-electrode system with a 6-M KOH aqueous solution as the electrolyte. The as-prepared composite was sandwiched between two pieces of nickel foam to work as the working electrode, a platinum foil (1 cm $\times$ 1 cm) was served as the counter electrode, and a Hg/HgO electrode was used as the reference electrode. The cyclic voltammetry (CV), galvanostatic charge and discharge test (GCD), and electrochemical impedance spectroscopy (EIS) measurements were performed by using a GHI660C electrochemical workstation (Shanghai Chenhua Instrument Company, China). A LAND battery program-control test system was employed to evaluate the cycling life of the working electrode.

3 Results and discussion

The morphology and microstructure of CCNF and NCCNF were investigated by SEM. From Fig. 1a, b, we can obviously find that CCNF was in uniform fiber structure, and the diameter of the fibers was about 300 nm. The surface of CCNF was not smooth, on which many nanoparticles were uniformly distributed formed from the decomposition of Co(Ac)$_2$ in the heat-treatment process. Figure 1c is the EDS of CCNF, which shows the existence of the Co and O elements, but the atomic ratio of O to Co is much smaller than 1:1, implying that the Co substance mostly exists in elemental Co metal and partly in CoO. In the inset of Fig. 1b, CCNF film is seen to be foldable, demonstrating an excellent mechanical flexibility. Figure 1d shows NiCo$_2$O$_4$ was grown on the surface of CCNF, and that the diameter of NCCNF was about 800 nm. Further, From Fig. 1e, NiCo$_2$O$_4$ was clearly seen to be in net-like structure. As shown in Fig. 1f, the EDS analysis reveals the presence of the C, O, Ni and Co elements in NCCNF, and that the atomic ratio of Ni to Co is estimated to be about 1.0:1.18, which shows the exist of Co and NiCo$_2$O$_4$. Due to the rigidity of the loaded NiCo$_2$O$_4$, NCCNF film is poorer in flexible performance than CCNF film. But the inset picture in Fig. 1e shows that NCCNF film can be bended to almost 180° in a bending radius of about 0.25 cm, meaning high mechanical flexibility.
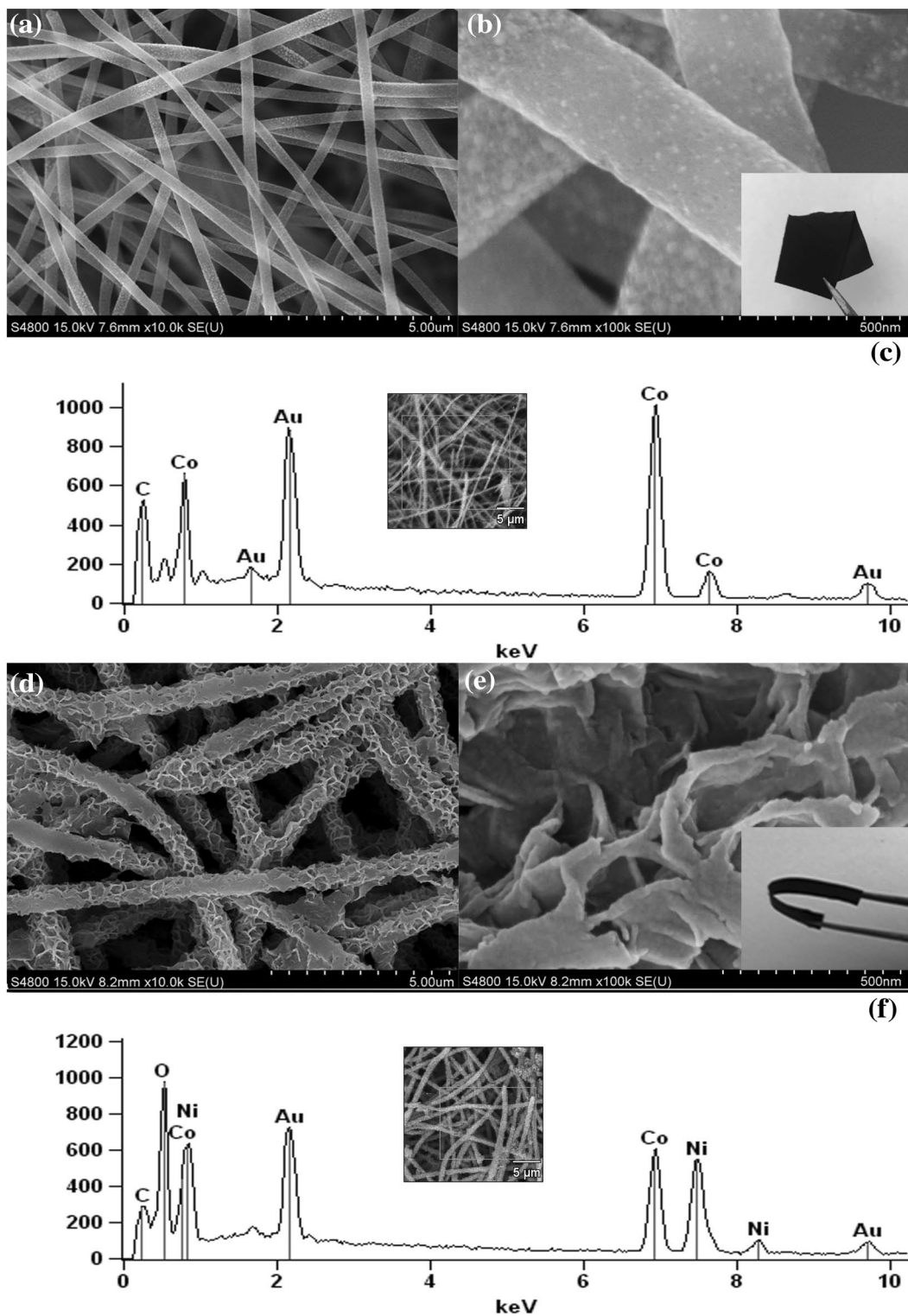
Fig. 1 **a**, **b** SEM images and **c** EDS spectrum of CCNF, **d**, **e** SEM images and **f** EDS spectrum of NCCNF. The insets in **b**, **e** are SEM images of CCNF and NCCNF films bended to almost 180°, respectively

The XRD and Raman methods were employed to study the crystal structure and composition of CCNF and NCCNF, and the spectra are shown in Fig. 2. In Fig. 2a, the XRD pattern of CCNF shows one obvious peak at 44.2° assigned to the (111) planes of Co (JCPDF No. 15-0806), indicating that the existence of Co metal within CCNF. This
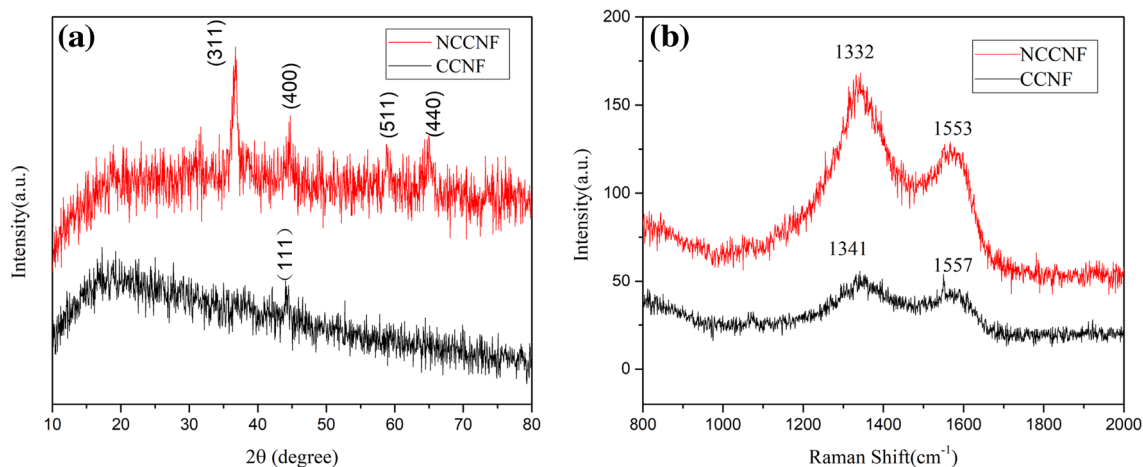
Fig. 2 **a** XRD pattern and **b** Raman spectroscopy of CCNF and NCCNF

demonstrates that the $Co(Ac)_2$ substance within the electrospun PAN-based nanofiber precursor was decomposed and most reduced to elemental Co metal. However, there is no diffraction peak from CoO, which means that the existed CoO is in amorphous state or implanted inside Co crystal texture in impurities. And the XRD pattern of NCCNF shows four obvious diffraction peaks at 36.7°, 44.4°, 59.1°, and 64.9°, which can be indexed to (311), (400), (511) and (440) planes of $NiCo_2O_4$ (JCPDF No. 73-1702), respectively, demonstrating that $NiCo_2O_4$ was successfully grown on the surface of CCNF through our hydrothermal technique. Raman spectroscopy is a powerful tool to characterize carbon-based materials. In Fig. 2b, we can see that the D bands were at 1332 or 1341 cm^{-1}, G bands were at 1553 or 1577 cm^{-1}. In general, D band is assigned to the structural defects and disorders of graphitic domains, whereas G band is attributed to the $E2_g$ mode of sp^2 carbon domains

explaining the degree of graphitization [34]. The relative intensity of the G and D band (I_G/I_D) is used to evaluate the degree of graphitization, and a high intensity ratio means high degree of graphitization [35]. The values of I_G/I_D for CCNF and NCCNF are 0.77 and 0.82, respectively, indicating the destruction of partial sp^3 defects and the rebuilt of sp^2 carbon during hydrothermal treatment.

To characterize the specific surface area and pore-size distribution of the samples, N_2 adsorption/desorption measurement was performed. Utilizing Brunauer–Emmett–Teller (BET) equation and Barrett–Joyner–Halenda (BJH) method, we can get that the BET surface area are 5.94 and 12.7 m^2 g^{-1} before and after the hydrothermal process, suggesting low pore degrees. The enlarged surface area from the hydrothermal process is a consequence of the net-like $NiCo_2O_4$ formed (seen in Fig. 1b, e). Figure 3b shows the pore-size distributions by BJH for CCNF and NCCNF.
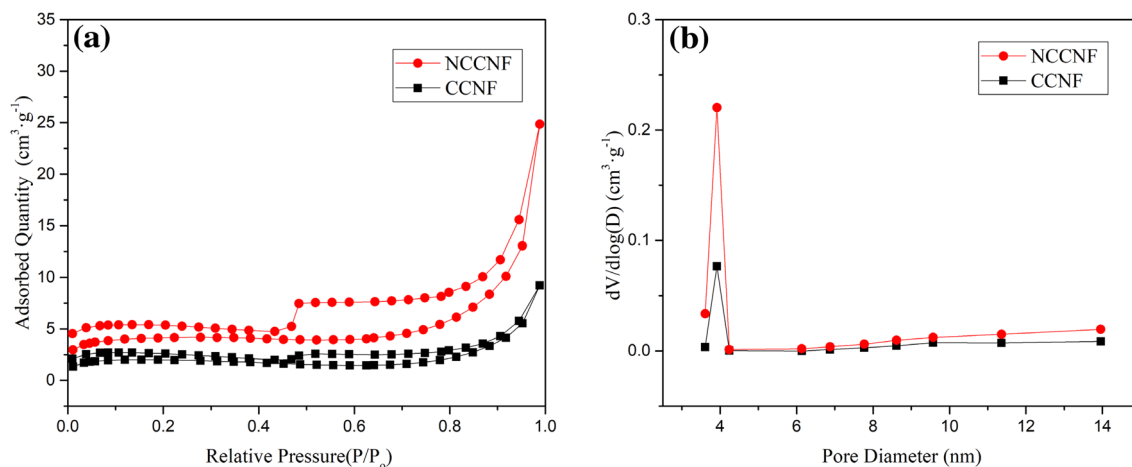

Fig. 3 **a** N_2 adsorption/desorption isotherms of CCNF and NCCNF, **b** pore-size distribution of CCNF and NCCNF

The pore size of CCNF and NCCNF are about 4 nm. The pores of CCNF are attributed to the decomposition of $Co(Ac)_2 \cdot 4H_2O$, whereas those of NCCNF are mostly owed to the net-like $NiCo_2O_4$.

The as-obtained products were directly employed as binder-free electrodes and their electrochemical properties were investigated in detail. Figure 4a, b show the CV curves

of CCNF and NCCNF at different scan rates (5, 10, 15, 20, and 25 mV s^{-1}). We can clearly see a pair of well-defined redox peaks within -0.15–0.35 V in every CV curve. This indicates that the capacitances of these two electrodes are distinct from electric double-layer capacitance characterized by nearly rectangular CV curves. A redox pair assigned to the quasi-reversible redox process of Co^{2+} to Co^{3+} appears
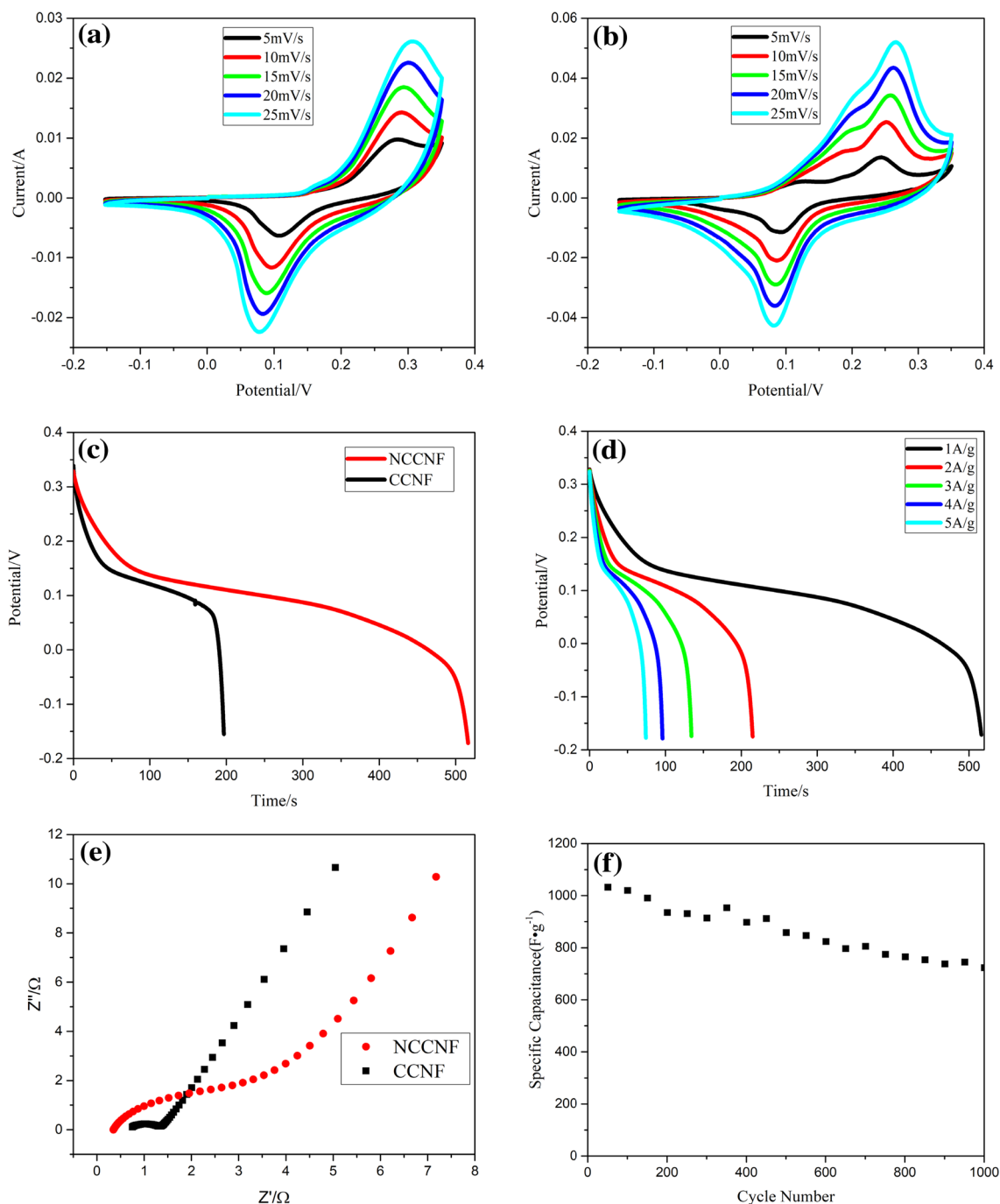
Fig. 4 **a** CV curves of CCNF, **b** CV curves of NCCNF, **c** GCD curves of CCNF and NCCNF at a current density of 1 A g^{-1}, **d** GCD curves of NCCNF at different current densities, **e** Nyquist plot of CCNF and NCCNF, **f** Cycling profiles of NCCNF at a current density of 1 A g^{-1}

in the region of 0.1–0.4 V for CCNF [36]. Compared to the CV curves of CCNF, those of NCCNF display double oxidation peaks, implying the appearance of the oxidation reaction from Ni^{2+} to Ni^{3+} [37, 38]. The specific capacitances of CCNF are 764, 565, 514, 478 and 450 F g^{-1}, while those of NCCNF are 1710, 1534, 1391, 1321, and 1267 F g^{-1} at scan rates of 5, 10, 15, 20 and 25 mV s^{-1}, respectively. The larger capacitance for NCCNF arises from the pseudocapacitive contribution of $NiCo_2O_4$ and the enlarged surface area caused by $NiCo_2O_4$. When the scan rate increases to 25 mV s^{-1}, the capacitance of NCCNF retains 74.1% of the initial value at 5 mV s^{-1}, revealing that NCCNF possesses a good rate capability. The GCD tests were also carried out to obtain the capacitance of CCNF and NCCNF, as shown in Fig. 4c. All the GCD curves have visible voltage plateaus, meaning their supercapacitive character. The capacitance of electrode materials can be calculated from the discharge time based on the following equation: $C_g = I\Delta t/m\Delta V$, Where $I, \Delta t, \Delta V$ and m are the discharge current (A), discharge time (s), voltage change during discharge (V) and mass of CCNF or NCCNF film (g), respectively. In Fig. 4c, d, we can clearly see that, compared to the 394 F g^{-1} of CCNF, the capacitance of NCCNF was up to 1032 F g^{-1}, revealing that its capacitance mostly comes from the contribution of $NiCo_2O_4$. The capacitance values of NCCNF calculated from GCD tests are 1032, 860, 804, 776 and 740 F g^{-1} at current densities of 1, 2, 3, 4 and 5 A g^{-1}, i.e., a capacitance retention of 72% can be calculated when the current density increases from 1 to 5 A g^{-1}. The decrease of the specific capacitance with increasing current is due to inadequate time for ions diffusion to the electroactive material surfaces. Compared with the previously reported $NiCo_2O_4$/CNTs co-doped carbon nanofibers (220 F g^{-1} at a current density of 1 A g^{-1}) [35] and $NiCo_2O_4$ wrapped by reduced graphene oxide (978 F g^{-1} at a scan rate of 5 mV s^{-1}) [39], our NCCNF presents a much higher capacitance. The high capacitance is attributed to a combination of the net-like porous structure of $NiCo_2O_4$ and the Co hybrid in the carbon matrix. The former provides a large $NiCo_2O_4$ surface area and a short ion diffusion paths to the interior surfaces, while the latter improves the electrical conductivity, which is proved subsequently by EIS.

The resistance behind the excellent capacitive performance of the CCNF and NCCNF electrode was investigated by EIS measurement. As shown in Fig. 4e, the plots all consist of a semicircle in the high-frequency region and a straight line in the low-frequency region. It is well known that the diameter of the semicircle corresponds to the charge transfer resistance, while the straight line in the low-frequency region is associated with the Warburg impedance, which can be attributed to the frequency dependence of ion diffusion and transport in the electrolyte [40]. The charge transfer resistance (R_{ct}) of CCNF and NCCNF are 0.658 and 2.94 Ω, respectively, these small values indicating that the

electron transfer velocity is fast between the electrode and the charge collector. The R_{ct} of NCCNF is 3.5 times higher than CCNF, which can be attributed to the poor electrical conductivity of $NiCo_2O_4$. Furthermore, the cycling stability of NCCNF was performed at a current density of 1 A g^{-1} and shown in Fig. 4f. The specific capacitance of NCCNF decreases to 723 F g^{-1} from initial 1032 F g^{-1} after 1000 cycles (i.e., about 70% of capacitance retention), suggesting a good cycling stability.

4 Conclusion

In summary, this work reports a flexible film electrode of $NiCo_2O_4$ grown on Co/C hybrid nanofibers (NCCNF) synthesized through electrospinning combining with carbonization and hydrothermal reaction. The as-prepared nanofiber film possesses an excellent mechanically flexible property and can be directly used as a binder-free working electrode. The targeted flexible film exhibits excellent electrochemical performance with a specific capacitance of up to 1710 F g^{-1} at 5 mV s^{-1} and an about 70% remain of the initial capacitance after 1000 cycles at 1 A g^{-1}, indicating great promising applications in flexible supercapacitors.

References

1. H. Zhao, C. Wang, R. Vellacheri, M. Zhou, Y. Xu, Self-supported metallic nanopore arrays with highly oriented nanoporous structures as ideally nanostructured electrodes for supercapacitor applications. Adv. Mater. **26**, 7654–7659 (2014)
2. I.E. Rauda, V. Augustyn, B. Dunn, Enhancing pseudocapacitive charge storage in polymer templated mesoporous materials. Accounts. Chem. Res. **46**, 1113–1124 (2013)
3. H.H. Li, J. Song, J.H. Zhou, W.J. Zeng, X.M. Feng, MoO_3 nanobelts/graphene nanocomposites: facile synthesis and application in supercapacitors. Chin. J. Inorg. Chem. **32**, 2041–2048 (2016)
4. B.T. Zhu, Z. Wang, S. Ding, Hierarchical nickel sulfide hollow spheres for high performance supercapacitors. RSC Adv. **1**, 397–400 (2011)
5. H. Sun, X. You, J. Deng, X.L. Chen, A twisted wire-shaped dual-function energy device for photoelectric conversion and electrochemical storage. Angew. Chem. **53**, 6664–6668 (2014)
6. J. Bae, M.K. Song, Y.J. Park, Fiber supercapacitors made of nanowire-fiber hybrid structures for wearable/flexible energy storage. Angew. Chem. **50**, 1683–1687 (2011)
7. W. Zeng, L. Shu, Q. Li, Fiber-based wearable electronics: a review of materials, fabrication, devices, and applications. Adv. Mater. **26**, 5310–5336 (2014)
8. S.W. Bian, L.L. Xu, M.X. Guo, F. Shao, S. Liu, Fabrication of graphene/cotton and MnO_2/graphene/cotton composite fabrics as flexible electrodes for electrochemical capacitors. Acta Phys.-Chim. Sin. **32**, 1199–1206 (2016)
9. R.S. Ingole, B.J. Lokhande, Electrochemically synthesized mesoporous architecture of vanadium oxide on flexible stainless steel for high performance supercapacitor. J. Mater. Sci.: Mater. Electron. **28**, 10951–10957 (2017)

10. C.L. Qin, Y.S. Zhang, Z.F. Wang, H.Q. Xiong, H. Yu, W.M. Zhao, One-step synthesis of CuO@brass foil by dealloying method for low-cost flexible supercapacitor electrodes. J. Mater. Sci.: Mater. Electron. **27**, 9206–9215 (2016)

11. B. Yao, L. Huang, J. Zhang, X. Gao, J.B. Wu, Y.L. Cheng, X. Xiao, B. Wang, Y. Li, J. Zhou, Flexible transparent molybdenum trioxide nanopaper for energy storage. Adv. Mater. **28**, 6353–6358 (2016)

12. B. Yao, J. Zhang, T.Y. Kou, Y. Song, T.Y. Liu, Y. Li, Flexible electrodes: paper-based electrodes for flexible energy storage devices. Adv. Sci. **4**, 1700107 (2017)

13. Z.Y. Xiong, C.L. Liao, W.H. Han, X.G. Wang, Mechanically tough large-area hierarchical porous graphene films for high-performance flexible supercapacitor applications. Adv. Mater. **27**, 4469–4475 (2015)

14. P. Wu, S. Cheng, L.F. Yang, Z.Q. Lin, X.H. Gui, Synthesis and characterization of self-standing and highly flexible δ-MnO$_2$@CNTs/CNTs composite films for direct use of supercapacitor electrodes. ACS Appl. Mater. Interface **8**, 23721–23728 (2016)

15. S.B. Chen, L. Wang, M.M. Huang, Reduced graphene oxide/Mn$_3$O$_4$ nanocrystals hybrid fiber for flexible all-solid-state supercapacitor with excellent volumetric energy density. Electrochim. Acta **242**, 10–18 (2017)

16. X.K. Ye, Y.C. Zhu, Z.H. Tang, In-situ chemical reduction produced graphene paper for flexible supercapacitors with impressive capacitive performance. J. Power Sources **360**, 48–58 (2017)

17. B. Yao, L.Y. Yuan, X. Xiao, J. Zhang, Y.Y. Qi, J. Zhou, Paper-based solid-state supercapacitors with pencil-drawing graphite/polyaniline networks hybrid electrodes. Nano Energy **2**, 1071–1078 (2013)

18. Y.Z. Zhang, T. Cheng, Y. Wang, W.Y. Lai, H. Pang, A simple approach to boost capacitance: flexible supercapacitors based on manganese oxides@MOFs via chemically induced in situ self-transformation. Adv. Mater. **28**, 5242–5248 (2016)

19. C. Xu, Z.H. Li, C. Yang, P.C. Zou, B.H. Xie, An ultralong, highly oriented nickel-nanowire-array electrode scaffold for high-performance compressible pseudocapacitors. Adv. Mater. **28**, 4105–4110 (2016)

20. Z.H. Pan, Y.C. Qiu, J. Yang, F.M. Ye, Y.J. Xu, Ultra-endurance flexibleall-solid-state asymmetric supercapacitors based on three-dimensionally coated MnOx nanosheets on nanoporous current collectors. Nano Energy **26**, 610–619 (2016)

21. L. Wang, X. Feng, L.T. Ren, Q.H. Piao, J.Q. Zhong, Flexible solid-state supercapacitor based on a metal-organic framework interwoven by electrochemically-deposited PANI. J. Am. Chem. Soc. **137**, 4920–4923 (2015)

22. X.Y. Fan, X.L. Wang, G. Li, A.P. Yu, Z.W. Chen, High-performance flexible electrode based on electrodeposition of polypyrrole/MnO$_2$ on carbon cloth for supercapacitors. J. Power Sources **326**, 357–364 (2016)

23. L.S. Zhang, Q.W. Ding, Y.P. Huang, H.H. Gu, Y.E. Miao, Flexible hybrid membranes with Ni(OH)$_2$ nanoplatelets vertically grown on electrospun carbon nanofibers for high-performance supercapacitors. ACS Appl. Mater. Interface **7**, 22669–22677 (2015)

24. Y.H. Chang, G.Y. Han, Y.Z. Chang, Flexible and compressible electrochemical capacitors based on polypyrrole/carbon fibers integrated into sponge. J. Alloys Compd. **708**, 1206–1215 (2017)

25. L. Li, Q.F. Zhong, N.D. Kim, G.D. Ruan, Y. Yang, Nitrogen-doped carbonized cotton for highly flexible supercapacitors. Carbon **105**, 260–267 (2016)

26. W.W. Li, F.X. Gao, X.Q. Wang, N. Zhang, M.M. Ma, Strong and robust polyaniline-based supramolecular hydrogels for flexible supercapacitors. Angew. Chem. Int. Ed. **55**, 9196–9201 (2016)

27. K. Wang, X. Zhang, C. Li, X.Z. Sun, Q.H. Meng, Chemically crosslinked hydrogel film leads to integrated flexible supercapacitors with superior performance. Adv. Mater. **27**, 7451–7457 (2015)

28. J. Li, E.H. Liu, W. Li, X.Y. Meng, S.T. Tan, Nickel/carbon nanofibers composite electrodes as supercapacitors prepared by electrospinning. J. Alloys Compd. **478**, 371–374 (2009)

29. Y.Z. Wu, R. Balakrishna, M.V. Reddy, A.S. Nair, B.V.R. Chowdari, Functional properties of electrospun NiO/RuO$_2$ composite carbon nanofibers. J. Alloys Compd. **517**, 69–74 (2012)

30. Y.L. Cheng, L. Huang, X. Xiao, B. Yao, L.Y. Yuan, T.Q. Li, Z.M. Hu, B. Wang, J. Wan, J. Zhou, Flexible and cross-linked N-doped carbon nanofiber network for high performance freestanding supercapacitor electrode. Nano Energy **15**, 66–74 (2015)

31. X. Chen, B.T. Zhao, Y. Cai, M.O.Z.P. Tade, Amorphous V-O-C composite nanofibers electrospun from solution precursors as binder- and conductive additive-free electrodes for supercapacitors with outstanding performance. Nanoscale **5**, 12589–12597 (2013)

32. J.L. Ge, G. Fan, Y. Si, J.X. He, H.Y. Kim, Elastic and hierarchical porous carbon nanofibrous membranes incorporated with NiFe$_2$O$_4$ nanocrystals for highly efficient capacitive energy storage. Nanoscale **8**, 2195–2204 (2016)

33. Y. Liu, J.Y. Zhou, L.L. Chen, P. Zhang, W.B. Fu, H. Zhao, Y.F. Ma, X.J. Pan, Z.X. Zhang, W.H. Han, E.Q. Xie, Highly flexible freestanding porous carbon nanofibers for electrodes materials of high-performance all-carbon supercapacitors. ACS Appl. Mater. Interface **7**, 23515–23520 (2015)

34. X.B. Wei, W. Chao, D. Peng, Z. Jiao, Z.Z. Cao, X.H. Xu, Synthesis of NiCo$_2$O$_4$ nanoneedle@polypyrrole arrays supported on 3D graphene electrode for high-performance detection of trace Pb^{2+}. J. Mater. Sci. **52**, 3893–3905 (2016)

35. N. Iqbal, X. Wang, A.A. Babar, Highly flexible NiCo$_2$O$_4$/CNTs doped carbon nanofibers for CO$_2$, adsorption and supercapacitor electrodes. J. Colloid Interface Sci. **476**, 87–93 (2016)

36. M. Li, L.B. Liu, Y.P. Xiong, Bimetallic MCo (M = Cu, Fe, Ni, and Mn) nanoparticles doped-carbon nanofibers synthetized by electrospinning for nonenzymatic glucose detection. Sens. Actuator B Chem. **207**, 614–622 (2015)

37. C. Yuan, J. Li, L. Hou, Ultrathin mesoporous NiCo$_2$O$_4$ nanosheets supported on Ni foam as advanced electrodes for supercapacitors. Adv. Funct. Mater. **22**, 4592–4597 (2012)

38. M. Yu, J. Chen, J. Liu, Mesoporous NiCo$_2$O$_4$ nanoneedles grown on 3D graphene-nickel foam for supercapacitor and methanol electro-oxidation. Electrochim. Acta **151**, 99–108 (2015)

39. S. Al-Rubaye, R. Rajagopalan, S.X. Dou, Z.X. Cheng, Facile synthesis of reduced graphene oxide wrapped porous NiCo$_2$O$_4$ composite with superior performance as an electrode material for supercapacitors. J. Mater. Chem. A **5**, 18989–18997 (2017)

40. B. Yang, L. .Yu, Q. Liu, The growth and assembly of the multi-dimensional hierarchical Ni$_3$S$_2$ for aqueous asymmetric supercapacitors. CrystEngComm **17**, 4495–4501 (2015)